

Article

Research on Optimization of Valley-Filling Charging for Vehicle Network System Based on Multi-Objective Optimization

Lingling Hu ¹, Junming Zhou ¹, Feng Jiang ^{1,2,3}, Guangming Xie ³, Jie Hu ¹ and Qinglie Mo ^{1,*}

¹ School of Mechanical and Automotive, Guangxi University of Science and Technology, Liuzhou 545006, China; 2002031@gxust.edu.cn (L.H.); a13078027926@163.com (J.Z.); 2011007@gxust.edu.cn (F.J.); 100001078@gxust.edu.cn (J.H.)

² Guangxi Huihuang Langjie Environmental Protection Technology Co., Ltd., Beihai 536000, China

³ Institute for Artificial Intelligence, Peking University, Beijing 100871, China; xiegming@pku.edu.cn

* Correspondence: 100001683@gxust.edu.cn

Abstract: Many electric vehicles connected to the grid will lead to problems such as poor stability of power grid generation. The key to solving these problems is to propose an efficient, stable, and economical valley-filling charging scheme for electric vehicles and grid users in the vehicle network system. Firstly, the convex optimization theory is used to make the grid achieve the optimization effect of valley filling. On this basis, the electricity price scheme with a time-varying coefficient as the variable is proposed to meet the single objective optimization of EV charging cost optimization, and its degree of influence on the grid valley-filling effect is analyzed. Secondly, based on the competitive relationship between EV charging cost and battery life, the P2D model is simplified and analyzed, and the attenuation law of battery capacity is quantitatively described. The multi-objective optimization problem is established to express in a Pareto matrix. Finally, the compatibility between the multi-objective optimization and grid valley charging is analyzed. The simulation results show that: (1) The convexity electricity price scheme can satisfy the requirements of various retention rates to achieve the valley-filling effect; (2) The filling effect is satisfied with the electricity price scheme that minimizes the charging cost, and the key factors affecting the filling effect are analyzed; (3) The multi-objective optimization scheme with charging cost and battery life is compatible with the valley-filling effect.

Keywords: vehicle network system; valley charging; P2D model; multi-objective optimization



Citation: Hu, L.; Zhou, J.; Jiang, F.; Xie, G.; Hu, J.; Mo, Q. Research on Optimization of Valley-Filling Charging for Vehicle Network System Based on Multi-Objective Optimization. *Sustainability* **2024**, *16*, 57. <https://doi.org/10.3390/su16010057>

Academic Editors: Surender Reddy Salkuti and Brian Azzopardi

Received: 26 November 2023

Revised: 16 December 2023

Accepted: 18 December 2023

Published: 20 December 2023



Copyright: © 2023 by the authors. Licensee MDPI, Basel, Switzerland. This article is an open access article distributed under the terms and conditions of the Creative Commons Attribution (CC BY) license (<https://creativecommons.org/licenses/by/4.0/>).

1. Introduction

With the increasing global environmental pollution and the depletion of fossil fuels [1], the transport sector in various countries is seeking a sustainable development path [2–4]. Electric vehicles (EVs) with zero emissions and high-efficiency conversions hold great promise [5–7]. With the increasing penetration rate of EVs [8], the charging problems faced have also been intensely studied [9,10]. The relevant research results prove that a large number of users tend to charge at 19:00 based on the disorderly charging scheme [11], superimposing the charging load based on the original load of the grid [12], resulting in the phenomenon of “Peak on Peak” [13], which significantly affects the stability of power grid generation [14]. The research location is a region in Guangxi, China, where the number of electric vehicles is large [15], and most small EVs have a maximum charging power of less than 8kW [16]. To cope with the increasing peak load demand [17], based on the interaction of all EVs in the region with the regional grid in the state of charging [18], the two are called “vehicle network systems”. In the system, the power grid is at the “Core level”, and the energy obtained by EV from the grid is at the “Carrier level” [19]. Most

of the existing research results are based on optimizing renewable energy sources [20–22], such as photovoltaic and wind power generation [23], to reduce the peak load of the grid or through the rational placement of fixed charging facilities for energy storage [24,25]. Habib et al. [26] proposed a method to simulate the operation effect of photovoltaic power generation as a static synchronous compensator to alleviate the peak load of the power grid. When the photovoltaic power generation system is connected to the power grid and the penetration rate is less than 25%, the simulation result of the total charging load of a day is reduced by 24.1%. Medved et al. [27] explored the impact of EV charging on the grid system and proposed an intelligent parking scheme to reduce the grid's peak load pressure. Simulation results showed that the project could improve the power generation stability of the grid. Ioakimidis et al. [28] provide scheduling EV charging and discharging processes for valley-filling optimization. Simulation results show that the total load of the power grid can be reduced by 3% and 20%, respectively, when the number of EVs is minimum and maximum. Abushnaf et al. [29] used a variety of electricity price schemes through the HEMS algorithm to monitor and reduce the user's power generation cost and the grid's total energy consumption in real time.

In the existing research results [30–32], the "Core level" valley-filling charging scheme to achieve the corresponding valley-filling effect depends on the extent to which the "Carrier level" gives up control of the charging curve. For "Carrier level" charging optimization, optimizing for multiple objectives based on the power of the charging curve is usually required. Therefore, for the study of valley-filling charging optimization of vehicle network systems, there is a structural contradiction between the power grid at the "Core level" and the electric vehicle at the "Carrier level" in the control of the charging curve, and few researchers have conducted research and analysis on this structural contradiction. There are also a few types of research on the influence of "Carrier level" multi-objective charging optimization on "Core level" filling charging optimization.

Therefore, this study attempts to conduct research from the above two perspectives, mainly based on three aspects of analysis: (1) "Core level" grid valley-filling charging optimization. This proposes a valley-filling charging strategy that can reduce power generation and has independent control. Based on convex optimization theory, the electricity price scheme is constructed to realize the effect of valley filling and charging; (2) "Carrier level" single-objective charging optimization. By analyzing the relationship between the charging curve and the electricity price scheme, three different time-varying coefficients $H(t)$ are proposed, and the best scheme is obtained by comparing and analyzing the valley-filling effect of the three electricity price schemes. At the same time, the degree of influence on the "core level" valley-filling charging effect is analyzed; (3) "Carrier-level" multi-objective charging optimization. By establishing and simplifying the battery durability mechanism model, the relationship between battery capacity decay and charging curve is quantitatively described, the charging cost and battery life are multi-objective optimizations, and the impact on the "Core level" filling charging optimization is also analyzed. Based on solving the structural contradiction of charge curve control in the vehicle network system, the proposed valley-filling charging scheme can achieve the valley-filling effect and achieve multi-objective optimization in the form of a Pareto front, which provides a reference value for the subsequent study of valley-filling charging optimization in the vehicle network system.

2. Numerical Approaches

2.1. Vehicle Network System Model and Definition

Figure 1, below, is a schematic diagram of the vehicle network system structure. In the vehicle network system, a large number of electric vehicles obtain energy from the power grid in a disorderly manner, resulting in a large number of charging loads gathering on the original load curve of the power grid in some periods, forming a peak load area, which makes the power grid bear a significant power generation cost. Usually, the power grid needs to coordinate and control the peak area by filling the valley to reduce the

power generation cost and improve the power generation stability. This section introduces and analyzes the vehicle network system model to lay the foundation for the subsequent original load curve and power generation cost model [33].

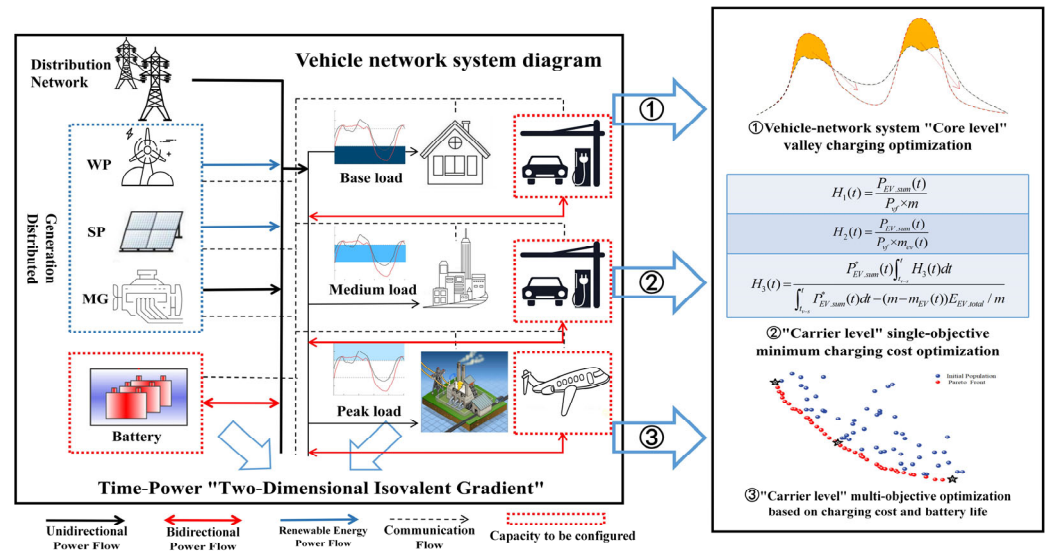


Figure 1. Vehicle network system structure diagram.

2.2. "Core Level" Grid Valley Charging Optimization

2.2.1. Original Load Curve and Generation Cost Model

Figure 2a is the original load curve of the regional power grid for the study, and its calculation theory is derived in [34]. Still, it only relates to the load situation of the regional power grid in the United States and is not universal. This paper will analyze the usage characteristics and conditions of the regional power grid based on the usage load in Guangxi, China. Figure 2b compares and examines the derivation process of the disorderly and orderly charging schemes. When the unordered charging scheme is adopted, the EVs reach their peak load at around 19:00. When the orderly charging scheme is adopted, the peak load of EVs is about 1:00 at night. The original load curve model can be verified by analyzing charging schemes proposed in several pieces of the literature [35,36], and quantitative research and comparison can be made for subsequent charging schemes.

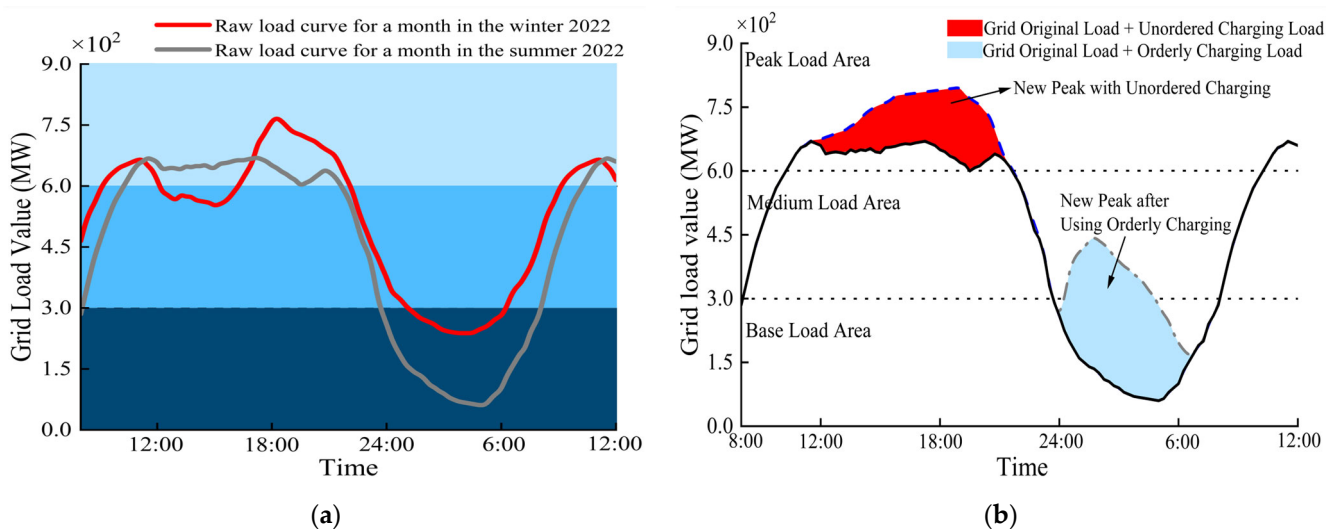


Figure 2. Load curves of different electricity price schemes in the study area. (a) Original load curves of the power grid; (b) Comparison curve of the two electricity price schemes.

This study uses a summer month as a case study, and the original load curve is usually predictive. Its power generation cost is a function of instantaneous power generation [37].

$$P_{gen.cost} = P_{gen.cost}(P) \quad (1)$$

In the above formula, $P_{gen.cost}$ is the power generation cost of the grid, $P_{gen.cost}(P)$ is the instantaneous power generation cost, and P is the instantaneous power generation. Power generation cost is one of the important indicators of power grid power generation efficiency. The higher the power generation cost, the lower the power generation efficiency, indicating the greater the need for energy efficiency optimization. The load curve in the figure is divided into three areas according to the size of baseload, intermediate load, and peak load, mainly based on the operating cost of power generation facilities. The power generation cost model is affected by fuel cost, and its convexity is also realized by the operating cost of power generation facilities, which is also the mainstream research strategy for the optimization of valley-filling charging. Convexity steady-state power generation cost is also adopted in this study, and its expression is as follows [38]:

$$\frac{d^2 P_{gen.cost}(P)}{dP^2} > 0 \quad (2)$$

2.2.2. Valley Charging

The “Core level” optimization goal of the vehicle network system is to control the charging curve P_{EV} of EVs in the region to minimize the total power generation cost in some periods. The optimization expression is as follows:

$$P_{EV.min} \int_{t_e}^{t_s} P_{gen.cost}(P(t)) dt \quad (3)$$

In the above formula, t_s and t_e are the beginning and end moments of the research period. Among them:

$$P(t) = P_{lc}(t) + P_{EV.sum}(t) \quad (4)$$

In the above formula, $P(t)$ is the total load of the power grid, which is the sum of the original load of the power grid and the total charging load of electric vehicles, and $P_{EV.sum}$ is the accumulation of the charging curves of all EVs. The optimization process is often affected by the SOC state of the battery, the charging power, and the state of the plug-in time. Therefore, for the total charging load of m electric vehicles, the charging load generated by electric vehicles is filled into the original load curve to minimize the power generation cost, which is discretized in time, and its Lagrange multiplier is obtained as follows:

$$P_{EV.total} = (\theta_{max}(m) - E(\theta_{plug-in}(m))E(P_{gen.cost.bat}(m)))M \quad (5)$$

$$L(P_{EV.sum}(t), \lambda, \nu) = \sum_{i=1}^m P_{gen.cost}(P_{lc}(t) + P_{EV.sum}(t))\Delta t \quad (6)$$

The above Formula (6) is simplified to:

$$P_{EV.sum} = \max[0, (P_{gen.cost})^{-1}(-\nu^*) - P_{lc}(t)] \quad (7)$$

In the above formula, $(P_{gen.cost})^{-1}$ is the inverse function of the derivation of the generation cost function $P_{gen.cost}$, so $P_{gen.cost}$ is a convex function, its derivation is monotonically increasing, and the inverse function must exist. Therefore, valley-filling (P_{VF}) is:

$$P_{VF} = (P_{gen.cost})^{-1}(-\nu^*) \quad (8)$$

The optimization expression of “Core level” grid valley charging in the vehicle network system and the corresponding valley optimization diagram are obtained:

$$P_{EV.sum}(t) = \max(0, P_{VF} - P_{lc}(t)), t \in (t_s, t_e) \quad (9)$$

The “Core level” grid valley-filling charging optimization solution achieved the valley-filling effect during the $[t - t_e]$ period, as can be seen from the Figure 3 below, without increasing the power generation infrastructure, the maximum EV retention rate in the region can be achieved by 50%. Regarding a 24% retention rate, the start time of valley filling is 0:00, the end time is 07:15, and the load power of valley filling is 2.6×10^2 MW. The best solution $P_{EV.sum}$ of the “Core level” filling charging optimization problem is a unique value, but the corresponding “Carrier level” EV charging curve combination P_{EV} can be variable. To achieve the effect of valley filling, the “Carrier level” is required to charge according to a specific charging curve, which is not universal and practical. The purpose of this research paper is to give “Carrier level” electric vehicles the control of the independent choice of charging curve and achieve a similar valley-filling effect:

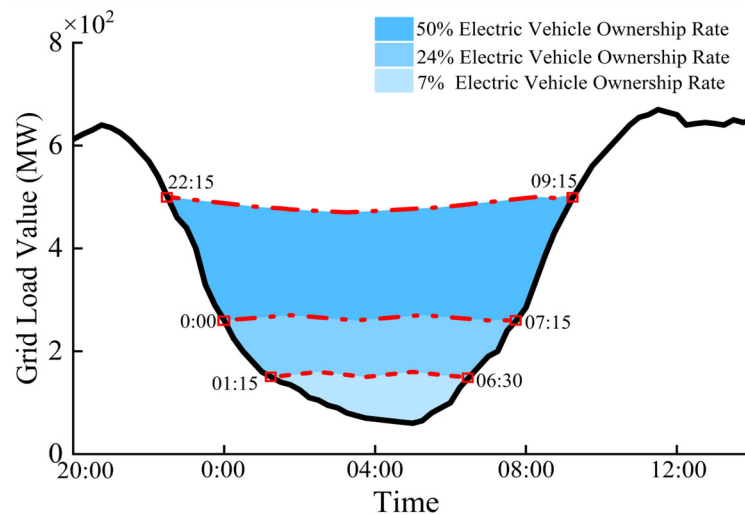


Figure 3. Grain-filling effect of three different electric vehicle retention rates.

2.3. Research on Single Objective Optimization of Three “Carrier Level” Electricity Price Schemes

In vehicle network systems, the goal of “Carrier level” EV single-objective charging optimization is to control the charging curve P_{EV} to minimize charging costs or maximize battery life [39]. The charging curve is mainly affected by the optimization objective, and most current research status is based on the minimum charging cost and the maximum battery life [40]. This study is also based on these two optimization objectives. As far as single-objective optimization is concerned, the charging cost optimization target with a better valley-filling effect of the “Core level” power system is selected for analysis. By studying the relationship between the charging curve and the electricity price scheme, the influence of three different electricity price schemes on the valley-filling effect is obtained [41].

The smart electricity price scheme in the power grid is one of the most effective schemes to optimize the charging energy efficiency [42]. It is mainly based on time-varying electricity prices and power prices, and the electricity price adjusts the grid load according to the charging time or charging power. In this paper, the two are integrated and unified, and a two-dimensional electricity price scheme varying with time t and power p is obtained, and its expression is:

$$f_{electrovalence} = f_{electrovalence}(t, p), t \in (t_{v-s}, t_{v-e}) \quad (10)$$

In the above formula, t_{v-s} ; t_{v-e} is the start and end time of valley filling, respectively, and the electricity price scheme is affected by time t and power p . Combined with the

convexity property of the above “Core level” power grid generation cost, the convexity of the electricity price scheme can be expressed as:

$$\frac{\partial^2 f_{\text{electrovalence}}(t, p)}{\partial P} > 0, t \in (t_{v-s}, t_{v-e}) \quad (11)$$

“Carrier level” electric vehicles control the charging curve to achieve the goal of minimizing charging costs, and when the battery SOC is full, the expression is:

$$P_{EV.\min} F_{EV}(m) = \int_{t_{e,m}}^{t_{s,m}} f_{\text{electrovalence}}(t, P_{EV}(t, m)) dt \quad (12)$$

In the above formula, $t_{s,m}$ and $t_{e,m}$ are the start and end charging times, respectively. Most drivers will choose to charge in the designated area before 0:00, so this study stipulates that all-electric vehicles are in the charging state before 0:00. After time discretization of the above problem, the Lagrange multiplier is as follows:

$$L(P_{EV}(t, m), \nu) = \sum_{i=1}^n f_{\text{electrovalence}}(t_i, P_{EV}(t_i, m)) \Delta t + \nu \left(\sum_{i=1}^n P_{EV}(t_i, m) \Delta t - D(m) \right) \quad (13)$$

where $t_1 = t_{s,m}$, $t_2 = t_{e,m}$, $D(m)$ is the charge battery power. And it is simplified to “constant electrovalence gradient condition”, expressed in the form of time continuity as:

$$\frac{\partial f_{\text{electrovalence}}(t_1, P_{EV}^*(t_1, m))}{\partial P_{EV}(t_1, m)} = \frac{\partial f_{\text{electrovalence}}(t_2, P_{EV}^*(t_2, m))}{\partial P_{EV}(t_1, m)}, t_1, t_2 \in (t_s, t_e) \quad (14)$$

In summary, Formula (14) can clearly describe the relationship between the electric price scheme of “Carrier level” EV with the minimum charging cost as the optimization objective and the charging curve, laying a foundation for the subsequent comparative study on the influence of the control electricity price scheme on the valley-filling effect [43].

2.4. “Carrier Level” Is Based on P2D Model Comparative Study

2.4.1. Electrochemical Equation of P2D Model

In the previous section, it has been described that the charging curve can be controlled autonomously at the “Carrier level”. At the same time, single-objective optimization can only be studied and analyzed from one optimization objective, which has certain limitations. This time, multiple optimization objectives, such as minimizing the charging cost and maximizing the battery life, will be studied and analyzed. At present, a large number of research studies indicate that the key to multi-objective optimization of “Carrier level” electric vehicles lies in the quantitative description of battery capacity attenuation degree based on the P2D model of battery durability [44]. The sandwich structure of the lithium-ion battery P2D model is shown in Figure 4 below, consisting of a negative electrode, a positive electrode, and a diaphragm. Positive and negative electrode materials are the “host” of lithium-ion batteries, and lithium ions are combined and separated from positive and negative electrode materials by embedding and de-embedding [45]. During the discharge of lithium-ion batteries, only lithium ions are allowed to pass through the diaphragm, so electrons pass through the external circuit from negative to positive. Lithium ions migrate from negative to positive through the diaphragm, and the SOC of the battery is reduced [46].

At the same time, the P2D model will be simulated and analyzed. Its mathematical model is expressed in Table 1 below, which is mainly composed of five equations describing the material distribution of the solid phase and liquid phase diffusion process in the r direction [47], the potential distribution in the x direction, and the lithium-ion embedding/de-embedding process on the two-phase interface respectively [48,49].

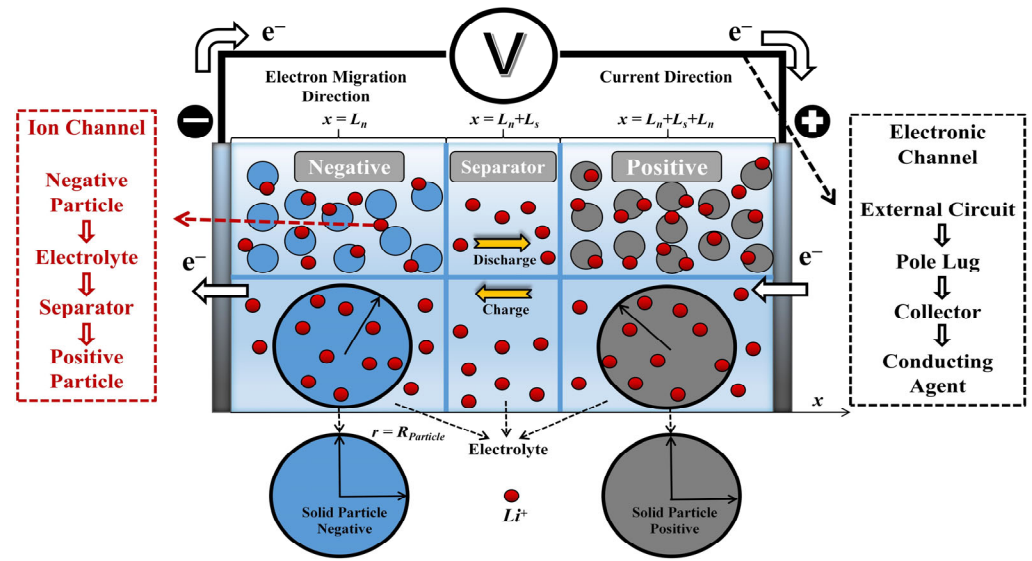


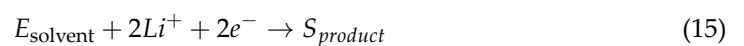
Figure 4. Lithium-ion battery P2D model sandwich structure diagram.

Table 1. Five equations of solid-liquid two-phase model for lithium-ion battery P2D.

Reaction Process	Formula	Boundary Condition
Liquid phase potential distribution (x direction)	$\varepsilon \frac{\partial c_1}{\partial t} = \nabla \cdot (D_{eff} \nabla c_1) + (1 - t_+) \frac{\nabla \cdot i_1}{F}$	$i_1 _{x=0} = i_1 _{l_p+l_s+l_n} = 0$ $i_1 _{x=l_p} = i_1 _{l_p+l_s} = I$ $c_1 _{t=0} = c_{1,0}$
Liquid phase material distribution (x direction)	$-k_{eff} \nabla \phi_1 + \frac{2k_{eff}RT}{F} (1 - t_+) (1 + \frac{d \ln f}{d \ln c_1})$	$i_1 _{x=0} = i_1 _{l_p+l_s+l_n} = 0$ $i_1 _{x=l_p} = i_1 _{l_p+l_s} = I$
Solid potential distribution (x direction)	$i_s = -\sigma_{eff} \nabla \phi_s$	$i_s _{x=0} = i_s _{l_p+l_s+l_n} = I$ $i_s _{x=l_p} = i_s _{l_p+l_s} = 0$
Solid phase material distribution (r direction)	$\frac{\partial c_s}{\partial t} = \frac{1}{r^2} \frac{\partial}{\partial r} (D_s r^2 \frac{\partial c_s}{\partial r})$	$\frac{\partial c_s}{\partial r} _{r=0} = 0$ $-FD_s \frac{\partial c_s}{\partial r} _{r=r_p} = \frac{R(x,t)}{a_n}$ $C_s _{t=0} = C_{s,0}$
B-V equation for solid-liquid two-phase interface	$R_n(x, t) = i_{0,s} a_n \left[\exp\left(\frac{\partial a F}{RT} \eta\right) - \exp\left(-\frac{\partial c F}{RT} \eta\right) \right]$	

2.4.2. Based on P2D Side Reaction Model

The main cause of lithium loss in recyclable lithium-ion batteries is mainly caused by the lithium-ion consumption of electrolyte interface film (SEI) and lithium precipitation. Lithium precipitation generally only occurs in overcharge, etc. At the same time, the growth of the negative SEI film appears in the entire life cycle of the battery, which is the key to the capacity decay of lithium-ion batteries [50]. Therefore, it is necessary to model and analyze the cell capacity attenuation mechanism model of negative SEI film growth. The electrons pass through the SEI film and react at the interface between the SEI film and the electrolyte. The side reaction can be expressed as:



In the formula, $E_{solvent}$ is the electrolyte solvent; the $S_{product}$ product of side reaction. On the surface of anode materials, it is generally considered that the side reaction is irreversible, so the side reaction rate is expressed by the Tafel equation:

$$R_s(x, t) = -i_{0,s} a_n \exp \left[-\frac{\alpha_{c,n} F}{H_g T} (\phi_s(x, t) - \phi_c(x, t) - U_s^{ref} - U_{film}(x, t)) \right] \quad (16)$$

In the above equation, $R_s(x,t)$ is the side reaction rate, $i_{0,s}$ is the equilibrium exchange current, and U_s^{ref} is the equilibrium potential, which can be seen to be similar to the expression of the main reaction overpotential. After the side reaction rate is obtained, the side reaction equation is as follows:

$$\int_0^{L_n} R_s(x,t) A dx = \frac{\alpha Q}{\alpha t} \quad (17)$$

In the above equation, Q is the total amount of recyclable lithium ions. This study mainly analyzes battery capacity attenuation. Recyclable lithium ion Q can be used to quantitatively characterize battery life status, and side reaction current density $R_s(x,t)$ can be used to quantitatively characterize battery life attenuation speed [51].

2.4.3. Comparative Analysis Based on P2D Model Simplification and Improvement

In the simulation process, the distribution and evolution process of various parameters inside the battery can be accurately explained by describing the electrochemical equation, and the battery attenuation mechanism and side reaction model of SEI film growth can be expressed in the form of the P2D model. However, it should be noted that the overall calculation is too large, and it is necessary to simplify the P2D model before the ‘‘Carrier level’’ multi-objective charging optimization. Based on the similarity of principal and secondary reactions in overpotential, the growth model of the P2D model can be simplified from a system of partial differential equations to a 0-dimensional algebraic model [52]. However, a large number of current studies show that the 0-dimensional algebraic model still has two major limitations: (1) Assuming that the distribution of matter in the potential distribution is uniform, which is a simplification based on the initial state, additional errors will be generated after the distribution of matter in the potential distribution is established; (2) The regional error of the larger equilibrium potential gradient of the negative active material also increases. To solve the above problems, this section will introduce the 0-dimensional algebraic model of resumes and put forward the method to improve it. It lays a foundation for subsequent comparative study and analysis of the P2D model, the 0-dimensional algebraic model, and the improved model.

The simplification of the 0-dimensional algebraic model mainly includes two simplification conditions: (1) The main reaction current density is independent of the x direction:

$$R_n(x,t) = \overline{R}_n = \frac{-i}{L_n A} \quad 0 < x < L_n \quad (18)$$

In the above formula, \overline{R}_n is the main reaction average current density, which can also be expressed when the charging current is i . Then, the expression of overpotential is obtained through the B–V equation of the main reaction. Based on the similarity of the principal and secondary reactions in overpotential, the following is obtained:

The core of the condition is that the side reaction current density is expressed as a function of the main reaction current density by an algebraic equation. The second simplified condition is as follows: (2) The concentration distribution of lithium ions in the solid phase is independent of the x direction, that is $C_s(x,t) = \overline{C}_s$, and \overline{C}_s is the average concentration of lithium ions in the solid phase. The main reaction equilibrium potential $U_n^{ref}(\theta_n(x,t))$ is a function of solid lithium ion concentration, then:

$$R_s(x,t) = -i_{0,s} a_n \exp\left(\frac{-U_s^{ref} - F(U_n^{ref}(\theta_n(x,t)))}{2R_g T}\right) \exp\left(-a \sinh\left(\frac{-i/AL_n}{2a_n i_0}\right)\right) \quad (19)$$

where the side reaction rate $R_s(x,t)$ is expressed as a function of the average SOC state $\bar{\theta}$ of lithium-ion concentration and the charging current i :

Because of the limitations of the 0-dimensional algebraic model mentioned above, an improved model is proposed. The first hypothesis in the 0-dimensional algebraic model,

that is, the main reaction rate is independent of x , is retained in the model, but the distribution of $U_n^{ref}(\theta_n(x, t))$ in the second hypothesis is studied, to achieve the purpose of model optimization. The liquid phase material distribution equation is expressed in the form of a non-homogeneous heat conduction equation to obtain the electrolyte concentration distribution. When other electrochemical parameters inside the battery remain constant, the lithium-ion concentration in the electrolyte also tends to a steady state. The equilibrium potential expression of the main reaction can be obtained, and finally, the improved model of the 0-dimensional algebraic model can be obtained:

$$R_s(x, t) = -i_{0,s} a_n \exp\left(\frac{-U_{ref,s} - F(U_n^{ref}(\bar{\theta}))}{2R_g T}\right) \exp\left(-\operatorname{asinh}\left(\frac{-i/AL_n}{2a_n i_0}\right)\right) \quad (20)$$

The 0-dimensional algebraic model and its improved model represent the side reaction model as a function of battery charging state θ and charging current i , which lays a foundation for the subsequent comparison of the performance of the three models and the multi-objective optimization of electric vehicles.

2.5. Research on Multi-Objective Optimization of “Carrier Level” eVs

Based on time t and power p , the two-dimensional scheme $f_{electrovalence}$ of “constant electricity price gradient” is constructed with the optimal charging cost as a single objective optimization. The charging cost of m electric vehicles is obtained by substituting the charging curve into the electricity price scheme. For the optimal battery life optimization goal, it is necessary to obtain a quantitative description of the capacity attenuation of lithium-ion batteries, and the charging curve is also obtained after substituting the battery attenuation characteristics [53]. The core of “Carrier level” electric vehicles is to optimize the best charging cost and the best battery life while optimizing the charging curve. There is a certain relationship between battery SOC and charging current, and the optimization of the charging current is also the optimization of the charging curve. The relationship between SOC and charging current is expressed as follows:

$$\frac{d\theta}{dt} = \frac{i(t)}{Q} \quad (21)$$

When the “Carrier level” electric vehicle takes into account the charging cost and battery life, it needs to optimize two or more objectives, which is called multi-objective charging optimization:

$$\min_{P_{EV}(t,m)} \left(\int_{t_s}^{t_e} R_{s,avg}(\theta(t), P_{EV}(t, m)) dt, \int_{t_s}^{t_e} f_{electrovalence}(t, P_{EV}(t, m)) dt \right) \quad (22)$$

$$\int_{t_s}^{t_e} P_{EV}(t, m) dt = D(m) \quad (23)$$

The optimization of battery life and charging cost in the expression of multi-objective optimization is realized by controlling the optimization variable $P_{EV}(t, m)$. Traditional multi-objective optimization needs to convert two objectives into a single objective optimization by weighted method, but there are some limitations. In this study, the unit inconsistency between charging cost and battery life cannot be solved in a weighted way. The competitive relationship between battery life and charging cost can be clearly expressed through the Pareto front, and multiple Pareto optimal solutions can be obtained at the same time, which is convenient for users to intuitively make charging decisions. The defi-

inition of the Pareto optimal solution is as follows: First, two objective functions of charging optimization will be proposed:

$$\begin{aligned} P_1(P_{EV}(t, m)) &= \int_{t_s}^{t_e} f_{electrovalence}(t, P_{EV}(t, m)) dt \\ P_2(P_{EV}(t, m)) &= \int_{t_s}^{t_e} R_{s,avg}(\theta(t), P_{EV}(t, m)) dt \end{aligned} \quad (24)$$

For a feasible solution $P_{EV}^*(t, m)$, if no other feasible solution $P_{EV}(t, m)$ exists, the following inequality is also true, the above formula, $P_{EV}^*(t, m)$ is the Pareto optimal solution in the multi-objective optimization problem.

$$\begin{cases} P_i(P_{EV}^*(t, m)) \geq P_i(P_{EV}(t, m)) & i \in 1, 2 \\ P_i(P_{EV}^*(t, m)) > P_i(P_{EV}(t, m)) & i \in 1, 2 \end{cases} \quad (25)$$

The methods of solving multi-objective optimization problems include genetic algorithms, ant colony algorithms, and particle swarm algorithms. In this study, a genetic algorithm, which is mature both in theory and application, is used to solve the multi-objective charging optimization problem. The algorithm flow is shown in the Figure 5 below:

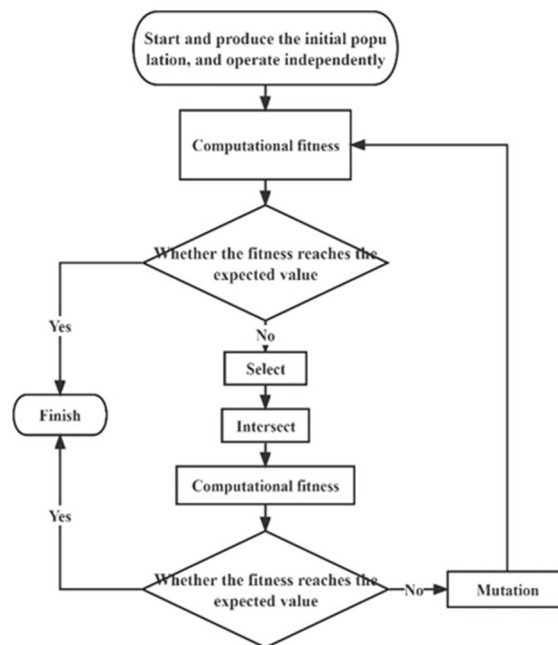


Figure 5. Genetic algorithm flow chart.

3. Result and Discussion

3.1. Comparative Analysis of Three Electricity Price Schemes

For electric vehicles in the “Carrier level” of the vehicle network system, the previous section studied and analyzed the single objective charging optimization with the best charging cost and obtained the relationship between the charging curve and the electricity price scheme. This section constructs three different electricity price schemes based on this research, aiming to achieve a valley-filling charging effect through all “Carrier level” electric vehicles under corresponding charging curves. First, the electricity price curve is constructed based on instantaneous power generation cost $P_{gen.cost}(P)$ curve:

$$f_{electrovalence}(t, P) = H(t)P_{gen.cost}\left(\frac{P}{H(t)}\right), t \in (t_{v-s}, t_{v-e}) \quad (26)$$

In the above equation, $H(t)$ is a time-varying coefficient, and the value is not constant. After substituting the electricity price scheme into the “constant electricity price gradient” of Formula (14):

$$\frac{\partial f_{electrovalence}(\frac{P_{EV}^*(t_x, m)}{H(t_x)})}{\partial(\frac{P_{EV}(t_x, m)}{H(t_x)})} = \frac{\partial f_{electrovalence}(\frac{P_{EV}^*(t_y, m)}{H(t_y)})}{\partial(\frac{P_{EV}(t_y, m)}{H(t_y)})}, t_x, t_y \in (t_{s, m}, t_{e, m}) \quad (27)$$

It is not difficult to find that the design difference of different electricity price schemes lies in the construction of different time-varying coefficients $H(t)$. This study will design three different $H(t)$ schemes to study their influence on the valley-filling effect, and the time-varying coefficient $H(t)$ should have the same trend as $P_{EV.SUM}(t)$, which can ensure that at the bottom of the valley, “Carrier level” electric vehicles can be charged at higher power. The specific three schemes are shown in Table 2 below, and the valley-filling effect under different $H(t)$ schemes is shown in the figure below. Based on the total charging load $P_{EV.total}$ of all-electric vehicles, the valley-filling effect is superimposed onto the original load curve P_{lc} to observe.

Table 2. Three electricity price schemes.

Option:	Formula	Distinction
$H_1(t)$	$H_1(t) = \frac{P_{EV.sum}(t)}{P_{vf} \times m}$	All vehicles
$H_2(t)$	$H_2(t) = \frac{P_{EV.sum}(t)}{P_{vf} \times m_{EV}(t)}$	At the time t for the charging state of the vehicle
$H_3(t)$	$H_3(t) = \frac{P_{EV.sum}^*(t) \int_{t_{v-s}}^t H_3(t) d\tau}{\int_{t_{v-s}}^t P_{EV.sum}^*(t) d\tau - (m - m_{EV}(t)) E_{EV.total} / m}$	Ignore the power demand of the vehicle leaving home early ($m - m_{EV}(t)$) at time t

Firstly, the $H_1(t)$ scheme is constructed, which is relatively easy to construct. All “Carrier level” eVs in the vehicle network system in this region can obtain corresponding charging curves according to the condition of “constant electricity price gradient”. In this scheme, all the charging loads generated by the “Carrier level” will be superimposed on the original load of the grid. The influence on the “Core level” filling effect is shown by the yellow line in Figure 6. From the local perspective, it can be seen that the load floating error is 14.9% compared with the full-filling effect. The reason for this phenomenon is that some electric vehicles will finish charging earlier or later than the expected setting time. These electric vehicles that end the charging state earlier than expected or delay arriving at the charging state will charge with a larger charging power to ensure that the electricity meets the demand of the day. Still, this result leads to a larger fluctuation in the valley-filling effect, which is poor. To obtain a better valley-filling effect, the second scheme, $H_2(t)$, is proposed, which replaces all-electric vehicles with vehicles that still maintain the charging state at time t to better accurately study the range of objects and reduce the impact of some electric vehicles ending the charging state in advance or reaching the charging state in delay, resulting in a poor valley-filling effect. The effect of this scheme on the “Core level” filling effect is shown by the green line in Figure 6. From a local perspective, it can be seen that the load floating error is reduced to 2.3% compared with the full-filling effect. Compared with the first scheme, it is optimized, but there is still a gap with the effect of full valley filling. At 4:00 and 6:00, there is a small range of fluctuations in the power grid. The main reason for this phenomenon is that the total charging demand of electric vehicles ($m - m_{EV}(t)$) that end or delay to reach the charging state is in the total charging load, although the electric vehicles that end or delay to reach the charging state are ignored. The third scheme, $H_3(t)$, is proposed. After deducting the electricity demand of the electric vehicle ($m - m_{EV}(t)$) that ends early or reaches the charging state late, the optimal $H_3(t)$ scheme is formed based on the analysis of the electric vehicle ($m_{EV}(t)$) that is still in the charging state based on the new charging curve. The effect of this scheme on the “Core level” filling effect is shown by the blue line in Figure 6. From a local perspective, it can be seen that the

load floating error is further reduced to 0.89% compared with the full-filling effect. Compared with the previous two schemes, the valley-filling effect is better. Although there are fluctuations in some moments, it meets the grid's valley-filling requirements.

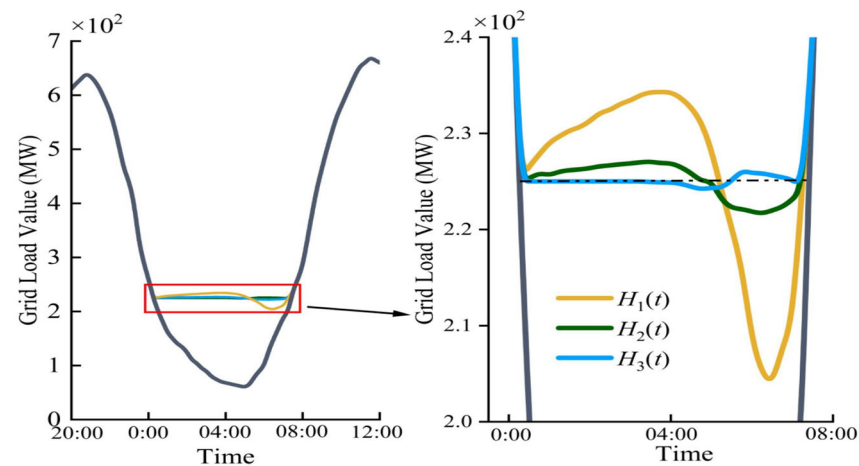


Figure 6. Three kinds of electricity price scheme grain filling effect.

To describe the factors affecting the valley-filling effect more intuitively, this section constructs a platform model composed of only three electric vehicles to simulate the electric vehicles in the entire vehicle network system. The valley-filling effect of the system composed of three electric vehicles is shown in the figure below. The time of the start and end charging states of the three electric vehicles is set at 0:00 and 8:00, respectively, to achieve the full valley-filling effect, as shown in Figure 7a. However, due to the delay of electric vehicle #3 reaching the charging state, the incomplete valley-filling effect, as shown in Figure 7b, or because electric vehicle #3 ends the charging state in advance, the incomplete valley-filling effect, as shown in Figure 7d. Figure 7c,e, respectively, remove electric vehicles that arrive late or end charging in advance based on the method of the third electricity price scheme to improve the effect of grid valley filling. Figure 7f shows the effect diagram of grain filling based on the third electricity price scheme after electric vehicle #3 reaches the charging state late and ends the charging state in advance. After deducting the total charging demand of the electric vehicle in the non-charging state at the corresponding time, a new original load curve is constructed, thus achieving the effect of nearly complete grain filling, as shown by the blue line in Figure 6.

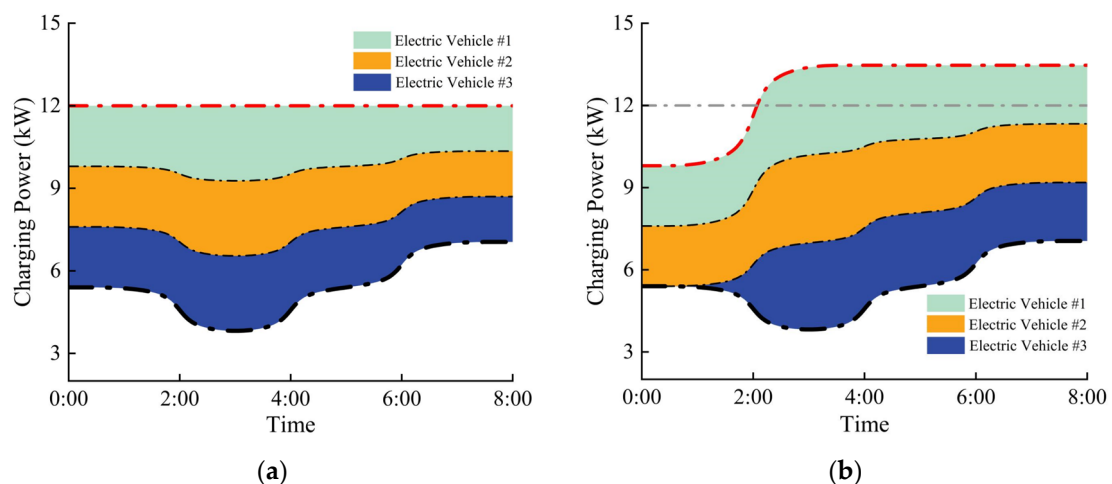


Figure 7. Cont.

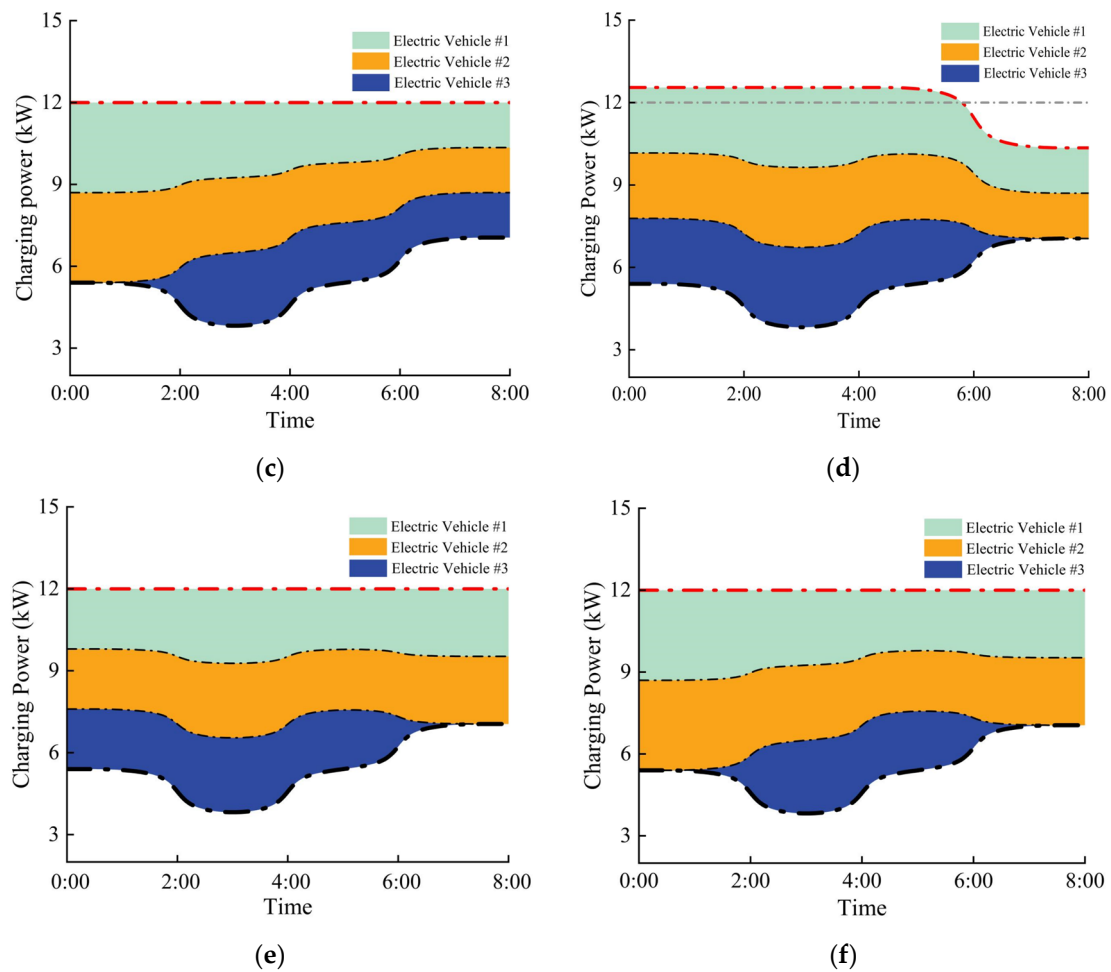


Figure 7. Three electric vehicles simulate three kinds of electricity price scheme grain filling effect: (a) full grain filling effect; (b) $H_1(t)$ electric vehicle #3 delay in reaching the charging state diagram; (c) $H_3(t)$ solution remove #3 delay after the grain filling effect; (d) $H_1(t)$ electric vehicle #3 early end charging state diagram; (e) $H_3(t)$ plan to remove #3 after the early end of the grain filling effect; (f) grain filling effect of $H_3(t)$ scheme.

3.2. Analysis of the Influence of “Carrier Level” Single Objective Optimization

The above research analyzes the optimization of valley-filling charging in the “Core level” power grid in the vehicle network system. It optimizes the charging cost through the single-objective optimization method of designing the electricity price scheme. To verify the stability of the proposed valley filling charging scheme, this section will conduct research and analysis from two dimensions, respectively: (1) There may be certain prediction errors between the original load curve and the charging state of electric vehicles in the “Core level” power grid system; (2) There may be errors in the execution ability of “Carrier level” electric vehicles for the three electricity price schemes formulated.

3.2.1. “Core Level” Grid Prediction Error

When there are original load curve prediction errors in the “Core level” or the “Carrier level” EV quantity m prediction errors in the vehicle network system, it will have a certain impact on the valley-filling charging effect. This research on the stability of the power grid system will be analyzed from three aspects: the deviation of the original load curve for 1 h, and the overestimation and underestimation of the number of electric vehicles m .

Figure 8 below shows the simulation result after predicting the deviation of the original load curve for one hour. The deviation of the original load curve will lead to the

deviation between the actual charging time of the electric vehicle and the charging time of the optimal filling effect, resulting in an incomplete filling effect.

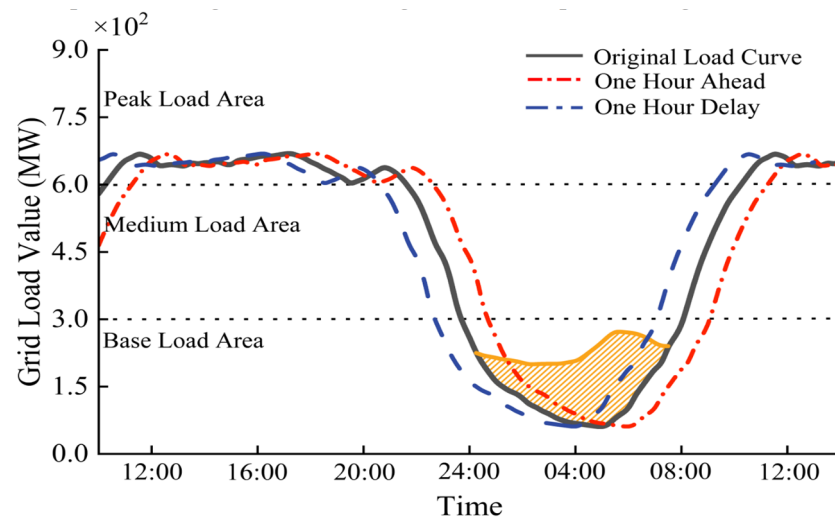


Figure 8. Prediction deviation diagram of the original load curve of the power grid.

Figure 9 below is the effect diagram of incomplete grain filling caused by the deviation of the predicted number of electric vehicles, m . Figure 9a shows that the number of electric vehicles m in the vehicle network system is underestimated by 30% of the true number ($m_1 = 0.7 m$). The assembly load generated by the actual number of electric vehicles in the power grid system will be 60% higher than the theoretical charging load. Compared with the full valley-filling effect, the charging load of some EVs will move from the two sides to the middle region, increasing the new peak load area by 19.6% based on the full valley-filling effect and further reducing the valley-filling time area. Figure 9b shows that the number of electric vehicles in the vehicle network system m is overestimated by 25% of the true number ($m_2 = 1.25 m$). The charging load generated by the actual number of electric vehicles in the system is 20% lower than the theoretical charging load. Compared with the full grain filling effect, the charging load of some EVs will move from the middle region to the two sides, reducing the new grain value load area by 11% based on the full grain filling effect and further extending the grain filling time area.

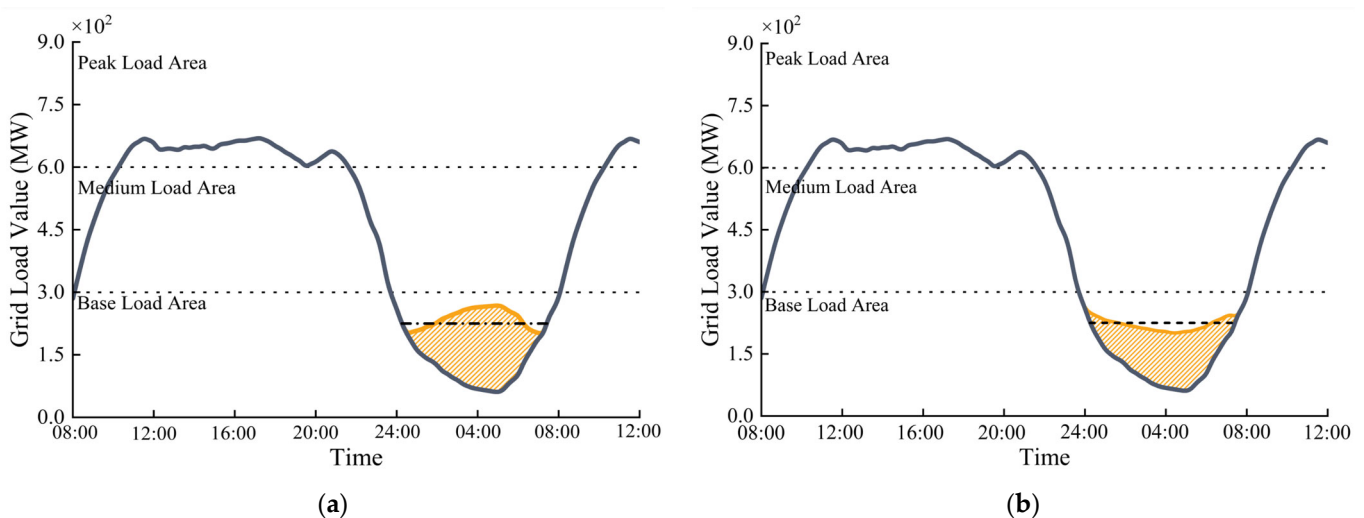


Figure 9. Prediction error chart of the number of electric vehicles in the vehicle network system. (a) Underestimating the number of electric vehicles m ; (b) Overestimating the number of electric vehicles m .

Table 3 below provides a quantitative analysis of the influence of the “Core level” prediction error on the valley-filling effect. First, the valley-filling charging scheme proposed in this paper is compared with the disorderly charging and orderly charging schemes proposed in [11,31]. Compared with the disorderly charging scheme, the generation cost of the valley filling charging scheme proposed in this paper is reduced by 30.7%, which effectively alleviates the problem of excessive peak load of the grid. At the same time, in terms of the “Core level” prediction error of the valley-filling charging scheme, it can be seen that the prediction error of the original load curve of the grid and the number of electric vehicles will increase the power generation cost and reduce the total profit of the grid, among which the original load curve error of the grid is the most obvious, the total profit of the grid is reduced by 10.2%, and the power generation cost is increased by 1.01%. In the case that the charging cost of electric vehicle users remains unchanged, the increased power generation costs are all borne by the grid. Therefore, in the long run, the power grid, as the “Core level” of the vehicle network system, should be improved in terms of the prediction accuracy of the number of electric vehicles and the prediction accuracy of the original load curve.

Table 3. Quantitative analysis of “Core level” prediction error on filling effect.

	Total Cost of Evs Generation Load (¥)	Total Charging Cost of EVs (¥)	Total Grid Profit (¥)
Unordered Charging	9.5819×10^4	-	-
Ordered Charging	6.8783×10^4	-	-
Valley-Filling Charging Effect (Article)	6.7428×10^4	7.5121×10^4	0.7690×10^4
Prediction Error 1 Hour (Figure 8)	6.8208×10^4	7.5121×10^4	0.6911×10^4
Underestimating the Number of EVs (Figure 9a)	6.7541×10^4	7.5188×10^4	0.7646×10^4
Overestimating the Number of EVs (Figure 9b)	6.7617×10^4	7.4876×10^4	0.7259×10^4

3.2.2. “Carrier Level” Electric Vehicle Execution Capability Error

There are errors in the execution ability of “Carrier level” electric vehicles in the vehicle network system for the three tariff schemes. Because the optimal charging curve of electric vehicles may be charged in a way that exceeds the maximum charging power in some periods, the effect of valley filling will be analyzed from the perspective of charging power difference.

Under daily circumstances, most of the electric vehicles in the grid system need to charge a large amount when they return to the charging facility, and the charging state ends late. However, in special cases, such as when the car needs a large amount of charging but the charging start time is early, the corresponding optimal charging curve may be charged with high power at some moments, which has an unstable impact on the valley-filling effect. The following figure is a simulation analysis of the impact of the maximum charging power of electric vehicles on the grid valley charging optimization. The difference is made based on the maximum charging power value. The results are shown in Figure 10 below. It is concluded that the greater the charging power, the smaller the impact on the grid valley charging optimization.

Table 4 below provides a quantitative analysis of the impact of the “Carrier level” execution capacity error on the valley-filling effect. It can be seen that although the power restriction leads to a fluctuation in the valley-filling effect and adds additional power generation costs to the grid, the variation is negligible. Under the three power limits, the total charging cost increased by 0.69%, 4.64%, and 23.07%, respectively, and the increase in grid profit was mainly borne by the total charging cost of electric vehicle users. Therefore, in the long run, “Carrier level” electric vehicles do not need to take corresponding measures from the error of their execution capacity.

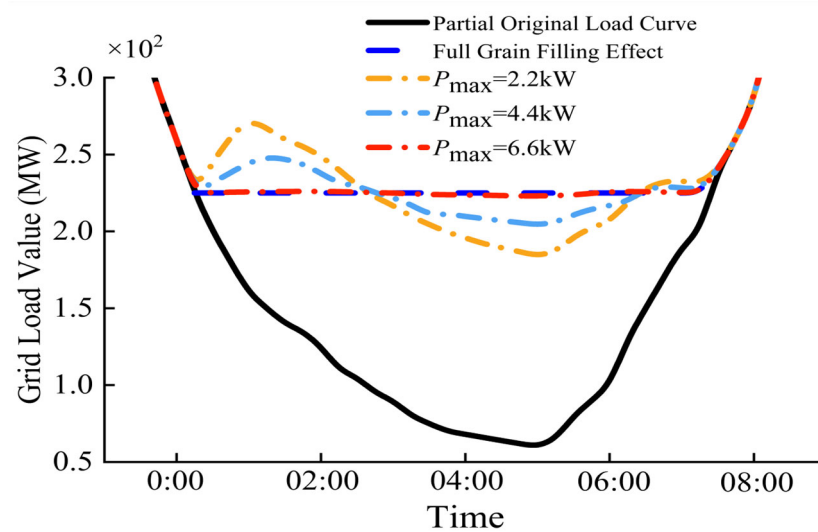


Figure 10. Effect of maximum charging power on valley-filling effect.

Table 4. Quantitative analysis of the effect of “Carrier level” execution ability error on the valley-filling effect.

	Total Cost of Evs Generation Load (¥)	Total Charging Cost of EVs (¥)	Total Grid Profit (¥)
No Power Limit Required Effect	6.7428×10^4	7.5121×10^4	0.7690×10^4
6.6 kW	6.7436×10^4	7.5638×10^4	0.8290×10^4
4.4 kW	6.7450×10^4	7.8603×10^4	1.1152×10^4
2.2 kW	6.7492×10^4	9.2455×10^4	2.4963×10^4

3.3. Comparative Analysis of the P2D Model and Improved Model Simulation

3.3.1. P2D Model Simulation Analysis

This study’s P2D model of the lithium-ion battery is expressed mathematically based on the partial differential equation in Table 1. In this section, the P2D model of the partial differential equations is first simulated and solved, laying the foundation for simplifying and improving the subsequent model.

The commonly used methods to solve this type of problem include the following: (1) Symbolic languages Map, Mathematica, GNU Octave, and MathCAD; (2) Compiled languages FORTRAN and C++; (3) Finite element simulation software such as Comsol 6.1, Ansys 2023R1, and Battery Design Studio v11.04. The advantage of using symbolic languages and compiled languages to simulate the P2D model is that the programming freedom is high, and the P2D model can be modified, or the algorithm can be improved to improve the solving efficiency. But the disadvantage is also obvious: it needs to invest a lot of time in learning programming methods and solving methods of partial differential equations. Commercial software has integrated the lithium-ion battery P2D model library, which can be used directly and can be co-simulated with MATLAB R2022a software. Therefore, COMSOL was chosen as the simulation tool. The simulation parameters of lithium-ion batteries are shown in Table 5.

Figure 11 is based on COMSOL 6.1 software to describe the five equations of the P2D model of lithium-ion batteries under typical working conditions and the main and side reaction current density distribution diagram, solid phase, and liquid phase potential and material distribution diagram under the Tafel equation. In the whole charging process, five moments (the 2000s, 2500s, 3000s, 3500s, and 4000s) were selected. Figure 11a,b shows the distribution of primary and secondary reaction current density in the x direction. As shown in Figure 11a, the simulation was under constant current charging conditions, so

the main reaction current density was constant in the x direction. In the 2000s, the main reaction rate of the outer side was significantly higher than that of the inner side, while in the 3000s, the main reaction rate of the inner side was higher than that of the outer side. Unlike the main reaction rate, the side reaction rate showed a certain regularity. As shown in Figure 11b, the inner side reaction rate was always higher than the outer side reaction rate at any time, and the side reaction rate everywhere increased with the increase of SOC. Figure 11c shows the cross-section of the distribution of the negative solid phase material in the x direction. It can be seen from the figure that the concentration of lithium ions in all parts of the solid phase increases with the passage of charging time, and the concentration on the outside is higher than that on the inside. As shown in Figure 11d, the solid phase potential also has the same properties as the trend of solid phase substance concentration. Due to the large solid phase conductivity, there is little difference between different electric potentials. As shown in Figure 11e,f, the material distribution and potential of ternary lithium-ion batteries in the liquid phase are more stable. The difference is smaller, and the ion concentration increases with the charging time, and the concentration on the outside is greater than that on the inside. It also lays a foundation for the simplified and improved comparative analysis of the P2D model based on liquid phase material and potential distribution in the following section.

Table 5. P2D model simulation parameters.

Parameter Name	Negative Electrode	Positive Electrode	Diaphragm	Unit
Active material	Graphite	NCA(LiNi _{0.8} Co _{0.15} Al _{0.05} O ₂)	LiPF ₆	-
L	5.5×10^{-5}	4×10^{-5}	3×10^{-5}	m
R_p	2.5×10^{-6}	2.5×10^{-7}	-	m
ε_s^{brugg}	0.384	0.42	-	-
ε_l^{brugg}	0.444	0.41	-	-
$Brugg$		1.5		-
c_s	30,555	48,000	-	mol/m ³
c_l	1200	1200	1200	mol/m ³
D_s	3.8×10^{-15}	1.0×10^{-15}	-	m ² /s
D_l	7.6×10^{-10}	7.6×10^{-10}	7.6×10^{-10}	m ² /s
κ_s	100	-	100	S/m
t_+		0.365		-
R		8.314		Jmol ⁻¹ K ⁻¹
T		298.15		K
F		9.6486×10^4		C/mol
a_a, a_c	0.5	0.5	-	-

3.3.2. Comparative Analysis Based on P2D Model, 0-Dimensional Algebraic Model, and Improved Model

At a specific temperature T , 31 constant-current charging simulations were performed between 0–3 C at step size 0.1 C to charge the battery SOC from 20% to 90%. The total time of the P2D model is 1.267×10^4 s, with an average of 408 s each time. The 31-time simulation analysis on the 0-dimensional algebraic model based on Matlab only takes 0.32 s, which greatly improves the running speed. Meanwhile, the 31-time simulation analysis on the proposed improved model also takes 44 s, which reduces the operational performance compared with the 0-dimensional algebraic model. However, for P2D models, the computational performance is also greatly improved. It is worth noting that although the 0-dimensional algebraic model meets the operational performance, some regions of the equilibrium potential will be in the “platform region” during simulation, resulting in a decline in the accuracy of the model.

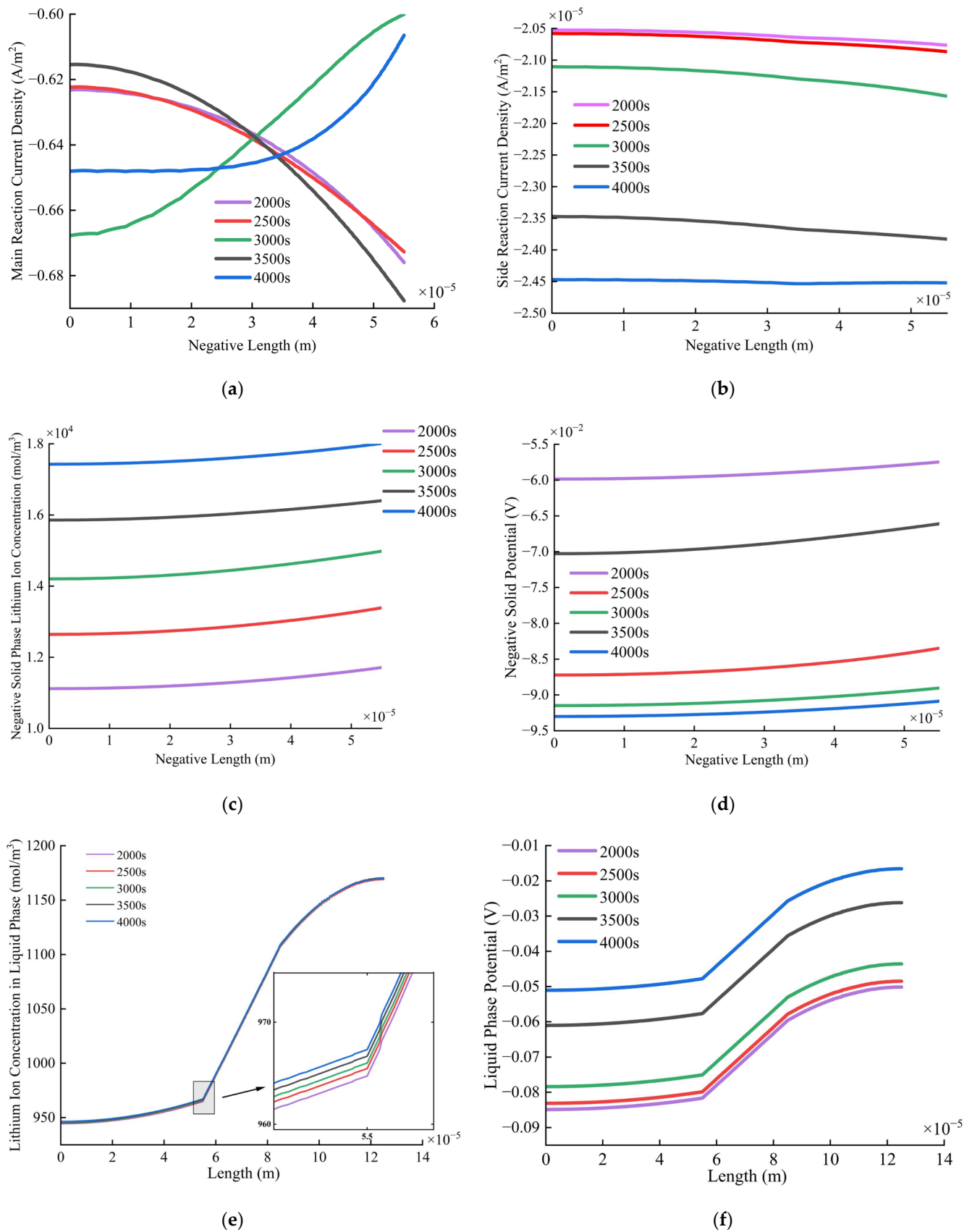


Figure 11. P2D model simulation results. (a) Main reaction current density; (b) side reaction current density; (c) negative solid phase material distribution; (d) negative solid-phase potential distribution; (e) distribution of substances in the liquid phase; (f) liquid phase potential distribution.

Figure 12 below compares the accuracy of the three models under 1C typical charging conditions. The figure shows that the improved model's average side reaction current density is consistent with that of the P2D model. When θ is near 0.5 and 0.8, the error fluctuation of simulation results of the 0-dimensional algebraic model and P2D model reaches 22%, while the error of the improved model is only 8%. The main reason is that there are two "platform regions" in the graphite negative equilibrium potential. The battery SOC state variable θ is a variable used to express the concentration of lithium ions in solid particles. Figure 13 shows the equilibrium potential diagram of graphite and hard carbon, and it can be seen that there is an obvious "Platform area" for graphite, and the equilibrium potential change in this region is not obvious. Compared with graphite, hard carbon does not have a "Platform area", and the equilibrium potential changes significantly.

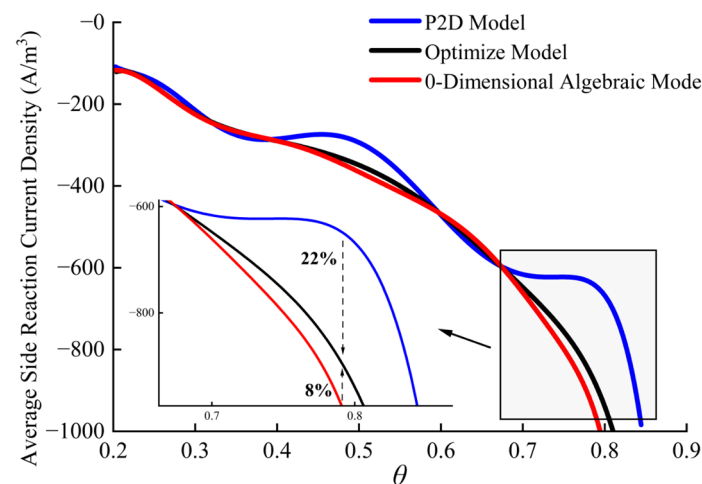


Figure 12. Comparison of simulation results of the three models' average negative side reaction current density.

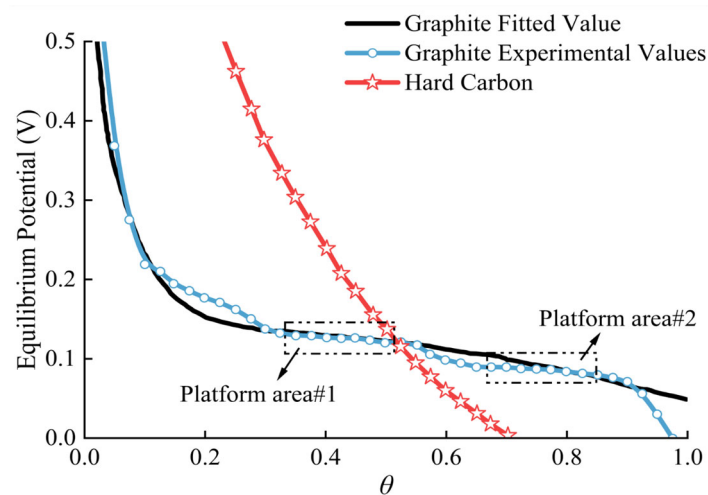


Figure 13. Schematic diagram of "Platform region" of equilibrium potential.

Under the operation mechanism of the 0-dimensional algebraic model, the average side reaction current density is determined by both the average equilibrium potential and the charging current. Under the constant current charging condition, the average SOC of the negative electrode is in the "Platform area" of the equilibrium potential curve, resulting in errors. When the P2D model and the improved model are carried out under the condition of constant charging current, the electrolyte substance and potential distribution region are in a certain steady state. The equilibrium potential distribution caused by the distribution of solid lithium ion concentration in the x direction must have an opposite trend to the potential distribution so that the equilibrium potential distribution avoids the

“Platform region”. This is why there is no “Platform region” for P2D models and their improved models.

To sum up, this section mainly simplified and improved the SEI film growth mechanism model based on the P2D model for comparative analysis, ensuring the accuracy requirements of the model and improving its operational performance so that it can achieve a quantitative description of the battery capacity, laying the foundation for solving the “Carrier level” multi-objective optimization problem in the next section. Compared with the traditional P2D model and 0-dimensional algebraic model, the proposed improved P2D model has better precision and computational performance.

3.4. Multi-Objective Optimization of “Carrier Level” and Influence Analysis on “Core Level” Valley Filling Charging

The multi-objective optimization problem has been explained in detail in Section 2.5. The multi-objective optimization problem of “Carrier level” in this section, as the extended part of the optimization of “Core level” valley filling and charging, is solved using a multi-objective genetic algorithm based on Matlab 6.1 software. The time step is 1 h, the population size is 100, and the Pareto optimization front is obtained after 37 iterations. As shown in Figure 14 below. Each point of the initial population and Pareto array corresponds to a different charging curve. The x -axis is the charging cost, and the y -axis is the added value of the equivalent resistance of the SEI film, which can more intuitively express the minimum charging cost and the best charging life performance. Each point corresponds to the degree of competition between the two, and when one optimization objective is improved, the other optimization objective must be weakened. The electric vehicle with charge control can choose the most favorable charging curve on the Pareto array based on its requirements. As shown in the figure below, Pareto#a represents the best charging cost and the worst battery life, and the degree of optimization of charging cost is slightly greater than that of single objective optimization. Theoretically, the optimization results of the two should be the same, and the main difference is that the simulation time of the two is different. The optimal solution of single-objective optimization is a subset of Pareto’s optimal solution of multi-objective optimization. Pareto#b represents a balance between charging cost and battery life, and Pareto#c represents the best battery life and the worst charging cost. The charging curves of the three are expressed in Figure 14. In Figure 14b, the charging curve with the best charging cost focuses on high-power charging in the valley period from 01:00–05:00, while the charging power is small in other periods. In Figure 14c, the charging curve with the best battery life moves backward, focusing on the valley time of 03:00–05:00 for high-power charging to achieve a lower SOC state of the battery and reduce the degree of battery attenuation. In Figure 14d, the charging curve, which takes into account charging cost and battery life, is somewhere in between.

“Carrier level” EV adopts multi-objective charging optimization, and after selecting the charging curve in the Pareto front, it is similar to single-objective optimization. There are certain errors in the execution ability of the electricity price scheme, which has an impact on the “Core level” grid valley-filling charging. As shown by the yellow line in Figure 15 below, compared with the theoretical effect of full valley filling, to reduce battery capacity attenuation, part of the electric vehicle load is moved from the left side of the valley to the right side. Although the “Carrier level” has caused an incomplete valley-filling effect and lower power generation efficiency, the increased cost is almost borne by the electric vehicle users themselves, and the total profit of the grid has not been reduced. It also shows that the “Core level” valley-filling charging can be effectively compatible with the “Carrier level” multi-objective charging optimization and better balance the conflict of interest between the “Core level” and “Carrier level” in the vehicle network system.

Table 6 below provides a quantitative analysis of the impact of “Carrier level” multi-objective charging optimization on the valley-filling effect. Although the multi-objective charging optimization results in an incomplete valley-filling effect, the increased power generation cost is negligible, the grid profit is increased, and most of the increase is borne

by EV users. At the same time, it also shows that the “Carrier level” multi-objective optimization charging can be compatible with the “Core level” valley filling charging optimization.

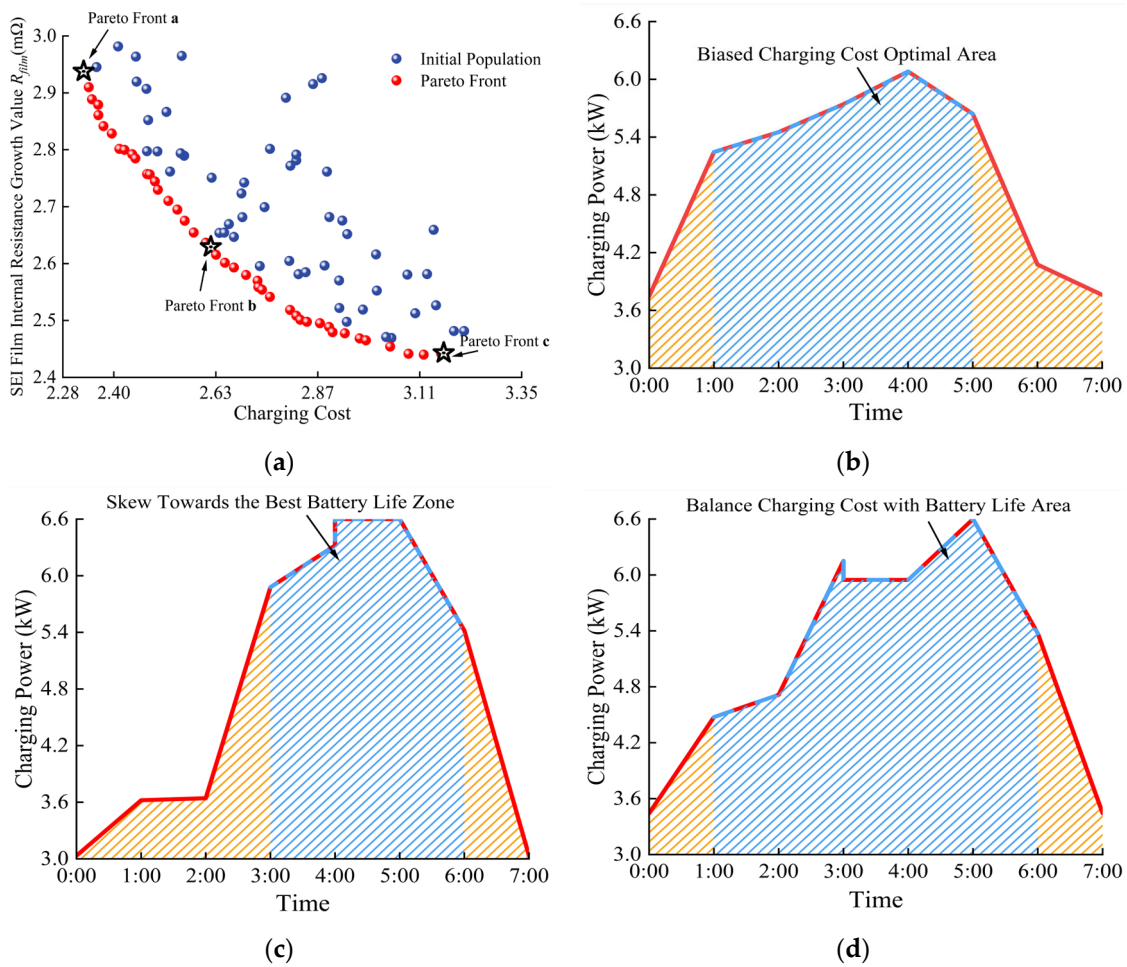


Figure 14. Pareto array for multi-objective optimization of “Carrier level” and corresponding charging curves. (a) Pareto array diagram; (b) focus on charging costs; (c) focus on battery life; (d) consider charging cost and battery life.

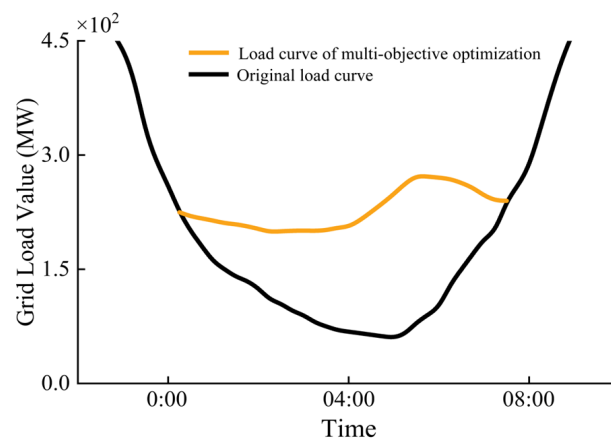


Figure 15. The influence of multi-objective optimization of “Carrier level” on grain filling effect.

Table 6. Quantitative analysis of the effect of “Carrier level” multi-objective charging optimization on valley filling.

	Total Cost of Ev Generation Load (¥)	Total Charging Cost of EV (¥)	Total Grid Profit (¥)
Unordered Charging	9.5819×10^4	-	-
Single Objective Optimization	6.7428×10^4	7.5121×10^4	0.7690×10^4
Multi-Objective Optimization	6.7553×10^4	8.7271×10^4	1.8835×10^4

4. Conclusions

Based on the phenomenon that a large number of electric vehicles are unordered and connected to the grid for charging, the research is carried out from two dimensions of “Core level” valley-filling assessing optimization and “Carrier level” multi-objective charging optimization to solve the problem of affecting the power generation stability after the formation of peak load period. The proposed valley-filling charging scheme solves the structural contradiction of charge curve control in vehicle network systems. For the “Core level”, the cost of the charging load is reduced by 30.7% compared with the disorderly charging, which meets the valley-filling effect. For the “Carrier level”, the scheme enables the user to control the charging curve and realizes the multi-objective optimization of charging cost and battery life through the Pareto matrix based on the quantitative description of the battery capacity decay degree. In addition, the feasibility and compatibility of each optimization scheme are quantitatively analyzed based on the three indexes of total power generation cost of the grid, total profit of the grid, and total charging cost of electric vehicles, and the following conclusions are obtained:

(1) The “Core level” is based on the convex optimization theory to achieve the valley-filling effect of electric vehicles under different retention rates. According to the law between the charging curve and the electricity price scheme, the electricity price scheme with the change of time coefficient $H(t)$ is constructed. Based on meeting the minimum charging cost at the “Carrier level” the valley-filling charging effect at the “Core level” is also achieved.

(2) In the case of the valley-filling charging scheme, the feasibility is analyzed from two aspects: prediction error and execution ability error. The simulation results show that the former increases the total power generation cost by 1.01%, and total profits were down 10.2%, the grid bears the increased cost of generating electricity. Therefore, optimizing the prediction accuracy of EV numbers and the total charging load of the power grid is necessary in the long run. The latter increased the charging cost by 0.69%, 4.64%, and 23.07%, respectively, under different power constraints, but total grid profits are up. It shows that the user bears the total cost of power generation, so there is no need to optimize it in the long run.

(3) “Carrier level” by establishing a P2D model for the quantitative description of battery capacity attenuation, the proposed optimization model is 14% more accurate than the 0-dimensional algebraic model. Based on the genetic algorithm, the battery life and charging cost were solved by multi-objective optimization, and the multi-objective optimization charging scheme was quantitatively analyzed. The simulation results show that although the scheme leads to an incomplete valley-filling effect and increases the total power generation cost, its profit does not decrease. Therefore, the increased cost is mainly borne by the user, showing that the proposed multi-objective optimization scheme is feasible based on charging facilities and is compatible with the “core level” valley-filling charging scheme.

(4) The “Core level” filling charging optimization and “Carrier level” multi-objective charging optimization jointly constitute the filling charging optimization system of the vehicle network system. In the follow-up study, we will continue to improve the factors affecting the effect of valley filling and improve the prediction accuracy of EV holdings and total power grid load in the study area for the “Core level”. For the “Carrier level”, the prediction accuracy of the battery capacity attenuation quantitative analysis model will

continue to be improved. The grid valley-filling effect can achieve the best result based on EV users' independent selection of charging optimization objectives.

Author Contributions: Conceptualization, L.H.; formal analysis, F.J. and J.Z.; software, L.H.; investigation, G.X. and J.Z.; resources, F.J.; writing—original draft preparation, J.Z. and F.J.; writing—review and editing, J.Z.; supervision, Q.M.; funding acquisition, J.H. and Q.M. All authors have read and agreed to the published version of the manuscript.

Funding: This work is supported by the Guangxi Key Research and Development Program project (Guike AB21220040), the National Natural Science Foundation of China (NO.6196300006), and the Guangxi University of Science and Technology Doctoral Fund Project (21Z34). This study was also supported by two independent research projects from the Guangxi Key Laboratory of Automotive Parts and Vehicle Technology, with project numbers 2022GKLACVTZZ02 and 2022GKLACVTZZ03.

Institutional Review Board Statement: Not applicable.

Informed Consent Statement: Written informed consent was obtained from all participants.

Data Availability Statement: All data used to support the findings of this study are included within the article.

Conflicts of Interest: Author Feng Jiang was employed by the company Guangxi Huihuang Langjie Environmental Protection Technology Co., Ltd. He is also a visiting scholar at the Institute of Artificial Intelligence, Peking University. The remaining authors declare that the research was conducted in the absence of any commercial or financial relationships that could be construed as a potential conflict of interest.

Nomenclature

B–V	Butler–Volmer
D(m)	Total Power to be Charged
EV	Electric Vehicle
E _{solvent}	Electrolyte Solvent
f _{electrovalence}	Electrovalence Scheme
HEMS	Home Energy Management System
H(t)	Time-varying coefficient
i _{0,s}	Equilibrium Exchange Current
L	Electrode length
m	Number of electric vehicles
P _{gen.cost}	Grid Generation Cost
P _{gen.cost} (P)	Instantaneous Cost of Grid Generation
P _{EV}	Charging Curve
P _{EV.sum}	Sum of Charge Curves
P _{VF}	Valley-Filling Charge Curve
P2D	Particle-to-Distributed
Q	Total amount of recycled lithium ions
R _n (x,t)	Main Reaction Rate
R _s (x,t)	Side Reaction Rate
SEI	Solid Electrolyte Interface
t _s /t _e	Study start/end
t _{v-s} /t _{v-e}	Start/end of Valley Filling
t _{s,m} /t _{e,m}	Charging start/end

References

1. Gabriel-Buenaventura, A.; Azzopardi, B. Energy recovery systems for retrofitting in internal combustion engine vehicles: A review of techniques. *Renew. Sustain. Energy Rev.* **2015**, *41*, 955–964. [[CrossRef](#)]
2. Tarroja, B.; Hittinger, E. The value of consumer acceptance of controlled electric vehicle charging in a decarbonizing grid: The case of California. *Energy* **2021**, *229*, 120691. [[CrossRef](#)]
3. Jenn, A.; Highleyman, J. Distribution grid impacts of electric vehicles: A California case study. *IScience* **2022**, *25*, 103686. [[CrossRef](#)] [[PubMed](#)]

4. Scicluna, K.; Azzopardi, B.; Spiteri, K. Power Quality Analysis for Light-Duty Electric Vehicles: A Case Study in Malta. *Energies* **2023**, *16*, 5673. [[CrossRef](#)]
5. Salkuti, S.R. Advanced Technologies for Energy Storage and Electric Vehicles. *Energies* **2023**, *16*, 2312. [[CrossRef](#)]
6. Hu, J.; Cao, W.; Jiang, F.; Hu, L.; Chen, Q.; Zheng, W.; Zhou, J. Study on Multi-Objective Optimization of Power System Parameters of Battery Electric Vehicles. *Sustainability* **2023**, *15*, 8219. [[CrossRef](#)]
7. Nour, M.; Chaves-Ávila, J.P.; Magdy, G.; Sánchez-Miralles, Á. Review of Positive and Negative Impacts of Electric Vehicles Charging on Electric Power Systems. *Energies* **2020**, *13*, 4675. [[CrossRef](#)]
8. Baraniak, J.; Starzyński, J. Modeling the Impact of Electric Vehicle Charging Systems on Electric Power Quality. *Energies* **2020**, *13*, 3951. [[CrossRef](#)]
9. Bibak, B.; Bai, L. An optimization approach for managing electric vehicle and reused battery charging in a vehicle to grid system under an electricity rate with demand charge. *Sustain. Energy Grids Netw.* **2023**, *36*, 1001145. [[CrossRef](#)]
10. Yang, A.; Wang, H.; Li, B.; Tan, Z. Capacity optimization of hybrid energy storage system for microgrid based on electric vehicles' orderly charging/discharging strategy. *J. Clean. Prod.* **2023**, *411*, 137346. [[CrossRef](#)]
11. Tian, J.; Lv, Y.; Zhao, Q.; Gong, Y.; Chun, L.; Ding, H.; Yu, Y. Electric vehicle charging load prediction considering the orderly charging. *Energy Rep.* **2022**, *8*, 124–134. [[CrossRef](#)]
12. Huang, Y.; Masrur, H.; Lipu, M.; Howladr, H.; Gamil, M.; Nakadmari, A.; Mandal, P.; Senjyu, T. Multi-objective optimization of campus microgrid system considering electric vehicle charging load integrated to power grid. *Sustain. Cities Soc.* **2023**, *98*, 104778. [[CrossRef](#)]
13. Zhan, K.; Hu, Z.; Song, Y.; Liu, N.; Xu, Z.; Jia, L. A probability transition matrix based decentralized electric vehicle charging method for load valley filling. *Electr. Power Syst. Res.* **2015**, *125*, 1–7. [[CrossRef](#)]
14. Ali, Z.M.; Calasan, M.; Aleem, S.H.E.A.; Jurado, F.; Gandoman, F.H. Applications of Energy Storage Systems in Enhancing Energy Management and Access in Microgrids: A Review. *Energies* **2023**, *16*, 5930. [[CrossRef](#)]
15. Zhang, L.; Sun, C.; Cai, G.; Koh, L. Charging and discharging optimization strategy for electric vehicles considering elasticity demand response. *eTransportation* **2023**, *18*, 100262. [[CrossRef](#)]
16. Ul-Haq, A.; Cecati, C.; Strunz, K.; Abbasi, E. Impact of Electric Vehicle Charging on Voltage Unbalance in an Urban Distribution Network. *Intell. Ind. Syst.* **2015**, *1*, 51–60. [[CrossRef](#)]
17. Liu, L.; Zhai, R.; Hu, Y.; Yin, H.; Wang, Q.; Xu, Y.; Sun, C. Capacity-Operation Collaborative Optimization for Wind-Solar-Hydrogen Multi-Energy Supply System. *Appl. Sci.* **2023**, *13*, 11011. [[CrossRef](#)]
18. Welzel, F.; Klinck, C.-F.; Pohlmann, Y.; Bednarczyk, M. Grid and user-optimized planning of charging processes of an electric vehicle fleet using a quantitative optimization model. *Appl. Energy* **2021**, *290*, 116717. [[CrossRef](#)]
19. Hossain, S.; Rokonuzzaman, M.; Rahman, K.S.; Habib, A.K.M.A.; Tan, W.-S.; Mahmud, M.; Chowdhury, S.; Channumsin, S. Grid-Vehicle-Grid (G2V2G) Efficient Power Transmission: An Overview of Concept, Operations, Benefits, Concerns, and Future Challenges. *Sustainability* **2023**, *15*, 5782. [[CrossRef](#)]
20. Ghirardi, E.; Brumana, G.; Franchini, G.; Perdichizzi, A. H₂ contribution to power grid stability in high renewable penetration scenarios. *Int. J. Hydrogen Energy* **2023**, *48*, 11956–11969. [[CrossRef](#)]
21. Bošnjaković, M.; Santa, R.; Crnac, Z.; Bošnjaković, T. Environmental Impact of PV Power Systems. *Sustainability* **2023**, *15*, 11888. [[CrossRef](#)]
22. Chiacchio, F.; D'Urso, D.; Aizpurua, J.; Compagno, L. Performance assessment of domestic photovoltaic power plant with a storage system. *IFAC-PapersOnLine* **2018**, *51*, 746–751. [[CrossRef](#)]
23. Montero, F.; Lamba, R.; Ortega, A.; Jahn, W.; Chen, W.; Guzmán, A. A bidirectional solar thermoelectric generator combining heat storage for daytime and nighttime power generation. *Appl. Therm. Eng.* **2023**, *224*, 119997. [[CrossRef](#)]
24. Mortaz, E.; Vinel, A.; Dvorkin, Y. An optimization model for siting and sizing of vehicle-to-grid facilities in a microgrid. *Appl. Energy* **2019**, *242*, 1649–1660. [[CrossRef](#)]
25. Das, H.; Rahman, M.; Li, S.; Tan, C. Electric vehicles standards, charging infrastructure, and impact on grid integration: A technological review. *Renew. Sustain. Energy Rev.* **2020**, *120*, 109618. [[CrossRef](#)]
26. Habib, M.; Gram, A.; Harrag, A.; Wang, Q. Optimized management of reactive power reserves of transmission grid-connected photovoltaic plants driven by an IoT solution. *Int. J. Electr. Power Energy Syst.* **2022**, *143*, 108455. [[CrossRef](#)]
27. Medved, D.; Bena, L.; Oliinyk, M.; Dzmura, J.; Mazur, D.; Martinko, D. Assessing the Effects of Smart Parking Infrastructure on the Electrical Power System. *Energies* **2023**, *16*, 5343. [[CrossRef](#)]
28. Ioakimidis, C.; Thomas, D.; Rycerski, P.; Genikomsakis, K. Peak shaving and valley filling of power consumption profile in nonresidential buildings using an electric vehicle parking lot. *Energy* **2018**, *148*, 148–158. [[CrossRef](#)]
29. Abushnaf, J.; Rassau, A.; Górniewicz, W. Impact of dynamic energy pricing schemes on a novel multi-user home energy management system. *Electr. Power Syst. Res.* **2015**, *125*, 124–132. [[CrossRef](#)]
30. Zhang, X.; Wang, Z.; Lu, Z. Multi-objective load dispatch for microgrid with electric vehicles using modified gravitational search and particle swarm optimization algorithm. *Appl. Energy* **2022**, *306*, 118018. [[CrossRef](#)]
31. Jian, L.; Zheng, Y.; Shao, Z. High efficient valley-filling strategy for centralized coordinated charging of large-scale electric vehicles. *Appl. Energy* **2017**, *186*, 46–55. [[CrossRef](#)]
32. Wang, X.; Jiang, B. Multi-objective optimization for fast charging design of lithium-ion batteries using constrained Bayesian optimization. *J. Power Sources* **2023**, *584*, 233602. [[CrossRef](#)]

33. Qu, Z.; Song, J.; Liu, Y.; Lv, H.; Hu, K.; Sun, J. Optimization Model of EV Charging and Discharging Price Considering Vehicle Owner Response and Power Grid Cost. *J. Electr. Eng. Technol.* **2019**, *14*, 2251–2261. [[CrossRef](#)]
34. Ahn, C.; Li, C.; Peng, H. Optimal decentralized charging control algorithm for electrified vehicles connected to smart grid. *J. Power Sources* **2011**, *196*, 10369–10379. [[CrossRef](#)]
35. Hu, Y.; Zhang, M.; Wang, K.; Wang, D. Optimization of orderly charging strategy of electric vehicle based on improved alternating direction method of multipliers. *J. Energy Storage* **2022**, *55*, 105483. [[CrossRef](#)]
36. Zhang, J.; Liu, J.; Zhang, X. Charging navigation strategy for electric vehicles considering empty-loading ratio and dynamic electricity price. *Sustain. Energy Grids Netw.* **2023**, *34*, 100987. [[CrossRef](#)]
37. Ma, S.; Yi, B.; Fan, Y. Research on the valley-filling pricing for EV charging considering renewable power generation. *Energy Econ.* **2022**, *106*, 105781. [[CrossRef](#)]
38. Khaki, B.; Das, P. Definition of multi-objective operation optimization of vanadium redox flow and lithium-ion batteries considering leveled cost of energy, fast charging, and energy efficiency based on current density. *J. Energy Storage* **2023**, *64*, 107246. [[CrossRef](#)]
39. Wang, R.; Mu, J.; Sun, Z.; Wang, J.; Hu, A. NSGA-II multi-objective optimization regional electricity price model for electric vehicle charging based on travel law. *Energy Rep.* **2021**, *7*, 1495–1503. [[CrossRef](#)]
40. Wang, T.; Jiang, Y.; Kang, L.; Liu, Y. Determination of retirement points by using a multi-objective optimization to compromise the first and second life of electric vehicle batteries. *J. Clean. Prod.* **2020**, *275*, 123128. [[CrossRef](#)]
41. Yang, Z.; Yang, F.; Min, H.; Tian, H.; Hu, W.; Liu, J. Energy management programming to reduce distribution network operating costs in the presence of electric vehicles and renewable energy sources. *Energy* **2023**, *263*, 125695. [[CrossRef](#)]
42. Zhu, W. Optimization strategies for real-time energy management of electric vehicles based on LSTM network learning. *Energy Rep.* **2022**, *8*, 1009–1019. [[CrossRef](#)]
43. Deng, J.; Hu, H.; Gong, S.; Dai, L. Impacts of charging pricing schemes on cost-optimal logistics electric vehicle fleet operation. *Transp. Res. Part D* **2022**, *109*, 103333. [[CrossRef](#)]
44. Zhang, S.; Andreas, N.; Li, R.; Zhang, N.; SUN, C.; Lu, D. Mitigating irreversible capacity loss for higher-energy lithium batteries. *Energy Storage Mater.* **2022**, *48*, 44–73. [[CrossRef](#)]
45. Shi, Q.; Liu, W.; Qu, Q.; Gao, T.; Wang, Y.; Liu, G. Robust solid/electrolyte interphase on graphite anode to suppress lithium inventory loss in lithium-ion batteries. *Carbon* **2017**, *111*, 291–298. [[CrossRef](#)]
46. Roy, A.; Patil, R.; Sen, R. The effect of fast charging and equalization on the reliability and cycle life of the lead acid batteries. *J. Energy Storage* **2022**, *55*, 105841. [[CrossRef](#)]
47. Jokar, A.; Rajabloo, B.; Desilets, M.; Lacroix, M. Review of simplified Pseudo-two-Dimensional models of lithium-ion batteries. *J. Power Sources* **2016**, *327*, 44–55. [[CrossRef](#)]
48. Li, Y.; Qian, K.; He, Y.; Kaneti, Y.; Liu, D.; Luo, D.; Li, H.; Li, B.; Kang, F. Study on the reversible capacity loss of layered oxide cathode during low-temperature operation. *J. Power Sources* **2017**, *342*, 24–30. [[CrossRef](#)]
49. Bermejo, R. Numerical analysis of a finite element formulation of the P2D model for Lithium-ion cells. *Numer. Math.* **2021**, *149*, 463–505. [[CrossRef](#)]
50. Vennam, G.; Sahoo, A.; Ahmed, S. A survey on lithium-ion battery internal and external degradation modeling and state of health estimation. *J. Energy Storage* **2022**, *52*, 104720. [[CrossRef](#)]
51. Liu, T.; Liu, C.; Liu, Y.; Sun, F.; Qiao, J.; Xu, T. Review on degradation mechanism and health state estimation methods of lithium-ion batteries. *J. Traffic Transp. Eng.* **2023**, *10*, 578–610. [[CrossRef](#)]
52. Gu, Y.; Wang, J.; Chen, C.; Xiao, W.; Deng, Z.; Chen, Q. A simplified electro-chemical lithium-ion battery model applicable for in situ monitoring and online control. *Energy* **2023**, *264*, 126192.
53. Silva, S.; Eckert, J.; Corrêa, F.; Silva, F.; Silva, L.; Dedini, F. Dual HESS electric vehicle powertrain design and fuzzy control based on multi-objective optimization to increase driving range and battery life cycle. *Appl. Energy* **2022**, *324*, 119723. [[CrossRef](#)]

Disclaimer/Publisher's Note: The statements, opinions and data contained in all publications are solely those of the individual author(s) and contributor(s) and not of MDPI and/or the editor(s). MDPI and/or the editor(s) disclaim responsibility for any injury to people or property resulting from any ideas, methods, instructions or products referred to in the content.